IEEE Photonics Journal
An IEEE Photonics Society Publication

All-Optical, All-Fibered Ultrafast Switching in 2-D InP-Based Photonic Crystal Nanocavity

Volume 2, Number 4, August 2010

M. Brunstein
A. M. Yacomotti
R. Braive
S. Barbay
I. Sagnes
L. Bigot
L. Le-Gratiet
J. A. Levenson

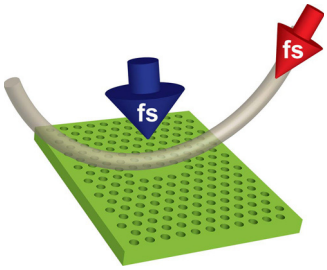

DOI: 10.1109/JPHOT.2010.2055841
1943-0655/$26.00 ©2010 IEEE

IEEE photonics SOCIETY
IEEE

All-Optical, All-Fibered Ultrafast Switching in 2-D InP-Based Photonic Crystal Nanocavity

M. Brunstein,[1] A. M. Yacomotti,[1] R. Braive,[1] S. Barbay,[1] I. Sagnes,[1] L. Bigot,[2] L. Le-Gratiet,[1] and J. A. Levenson[1]

[1]Laboratoire de Photonique et de Nanostructures (CNRS UPR20), 91460 Marcoussis, France
[2]Laboratoire de Physique des Lasers, Atomes et Molécules (CNRS UMR8523), Université Lille1, IRCICA, 59658 Villeneuve d'Ascq Cedex, France

DOI: 10.1109/JPHOT.2010.2055841
1943-0655/$26.00 ©2010 IEEE

Manuscript received May 11, 2010; revised June 24, 2010; accepted June 25, 2010. Date of publication June 28, 2010; date of current version July 19, 2010. These results are within the scope of C'Nano IdF and were supported by the Région Ile-de-France. C'Nano IdF is a CNRS, CEA, MESR and Région Ile-de-France Nanosciences Competence Center. Corresponding author: A. M. Yacomotti (e-mail: Alejandro.Giacomotti@lpn.cnrs.fr).

Abstract: The ultrafast optical switching capabilities of an InP-based photonic crystal cavity with quantum dots (QDs) are studied. The signal is evanescently coupled into the cavity at 1.5 μm through a tapered fiber. Both surface and fiber-coupled pumping schemes are investigated and compared. It is shown that the carrier-induced nonlinear response allows the signal to be switched within time windows ranging from a few picoseconds to 20 ps for the switch ON process and from 30 to 170 ps for the switch OFF process depending on the pumping configuration and power level. The carrier-induced nonlinear effects in the bulk, the wetting layer, and the QDs are discussed and compared. From a fit of the switching dynamics to the solutions of a rate equation for carrier relaxation, we show that the main contribution to carrier dynamics governing the switching processes comes from both nonradiative and radiative carrier recombination within the InAsP wetting layer.

Index Terms: Integrated nanophotonic systems, photonic crystals (PCs), semiconductor materials, ultrafast nonlinear processes.

1. Introduction

The ultrafast carrier-induced nonlinear response constitutes one of the major assets of semiconductor photonic crystals (PCs) for applications associated with the generation and manipulation of optical signals. Active PCs allow efficient integration and miniaturization of optical functions and can be optimized to operate either with high bandwidths or high wavelength selectivity through sharp optical resonances. In this context, InP PCs are intensely investigated due to their large carrier-induced nonlinearities that are compatible with gain/lasing operation at telecom wavelengths.

All-optical ultrafast switches with chip-integration compatibility and efficient coupling to the external environment are at the heart of high-speed communications. Optical switches based on 2-D photonic crystals (2DPCs) have already been proposed and investigated in III–V semiconductor-based materials in several configurations, including surface-resonant Bloch modes of a non-defective 2DPC, waveguides, and cavities [1]–[9]. The latter are usually coupled by means of end-fire configurations which require microscope objectives. An alternative road, which allows all-fibered devices with high coupling efficiency, is the evanescent coupling via a tapered fiber [10]–[13]. By contrast to on-chip waveguiding, this approach is restricted neither by the photonic bandgap nor

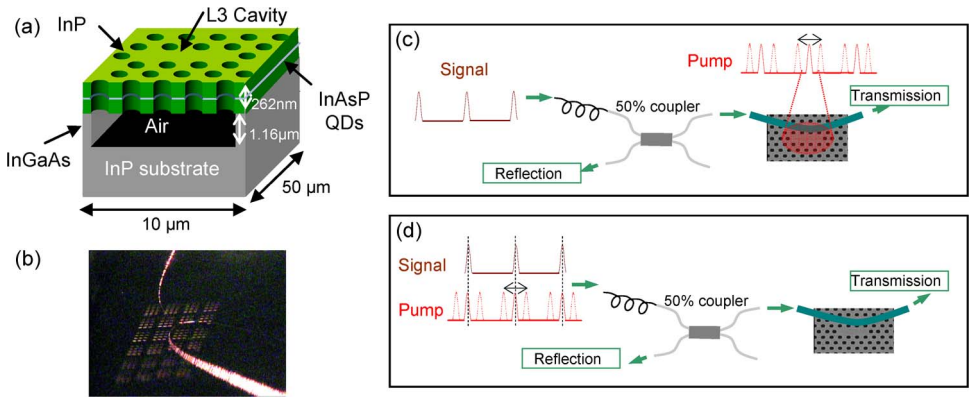

Fig. 1. (a) Sketch of the PC sample showing the L3 cavity. (b) Image of the whole sample and the fibered taper. (c) Experimental setup scheme for surface pump. (d) Experimental setup for all-fibered measurements. A non-represented translation stage allows a delay of the probe with respect to the pump. In (c) and (d), an SEM image of the L3 cavity is shown.

by the material absorption and allows enlargement of the range of wavelengths for the control and signal beams. Furthermore, it avoids the need for an additional coupling between the on-chip waveguide and an external system. Recently, fast switching capabilities of a PC nanocavity were investigated using an evanescent coupling through a tapered fiber. A ~2 ns, ON-OFF switching time was demonstrated [14]. The performance and resolution were limited by the pulse duration and the detection bandwidth, respectively. Indeed, the carrier-induced nonlinear response is expected to allow ON-OFF switching times shorter than 2 ns at least by one order of magnitude [4]. In this paper, we present pump and probe measurements with a 100-fs time resolution for all-fibered and surface pumping configurations in an InP-based 2DPC nanocavity.

2. Sample and Experimental Setup Description

The 2DPC is a triangular array of air holes lattice etched into a 10 $\times$ 50 μm InP-based suspended membrane. The period, the holes diameter, and the membrane thickness are a = 400 nm, d = 176 nm, and 262 nm, respectively. An L3 nanocavity (three missing holes) with the two end holes shifted away by 0.15a [see Fig. 1(a)] is located in the center of the 2DPC [15]. The InP membrane has a single layer of self-assembled InAsP/InP quantum dots (QDs), whose luminescence at 300 K is centered around 1.55 μm. The whole structure, incorporating an InGaAs sacrificial layer under the InP, is grown by metal–organic chemical vapor deposition (MOCVD). We point out that our system contains three different semiconductor structures, all of them potentially contributing to index changes as a function of injected carriers: the (3-D) InP slab, a (2-D) InAsP wetting layer (WL), and the (0-D) InAsP QDs. The wavelengths corresponding to their electronic bandgaps (λ_g) are 0.92, 1.1 and 1.55 μm, respectively. Since the wavelength of probe photons is $\lambda = 1490$ nm, the distances in wavelength to each λ_g are 570, 390, and 60 nm, respectively. In Section 5, the contribution of each semiconductor structure to carrier-induced nonlinear effects at the probe wavelength will be discussed.

In what follows, both the characterization of the nanocavity mode and the determination of the temporal response of the switch are performed by evanescently coupling a probe beam (the signal) into the nanocavity through a tapered optical fiber [see Fig. 1(b)]. The fiber taper (diameter of ~1.5 μm) is bent (radius of curvature ~500 μm) in such a way that the curved segment approaches the PC. Such U-shape-configuration reduces contact losses (leakage and absorption) outside the PC. Light is injected into the optical taper after propagating through a 7-m-long telecom single-mode optical fiber. The best coupling is obtained when the taper is in contact with the cavity allowing both low contact losses (1.6 dB) and mechanically robust and stable operation with no servo control.

The fibered taper is placed at the center of the cavity using a nano-positioning stage. The polarization angle is changed by means of a fibered polarization controller to optimize the optical coupling. An estimation of the coupling efficiency, calculated from the transmitted signal according

to reference [11], gives 44%, meaning that the high stability of the contact-mode operation is compatible with high coupling efficiency to the cavity mode. In addition to fiber-transmission measurements, the reflected signal upon interaction with the PC cavity is also measured using a 50% fibered coupler connected to the taper [see Fig. 1(c) and (d)]. Finally, an optical spectrum analyzer is used to spectrally resolve the changes in the transmitted/reflected signals.

In order to achieve sub-ps time resolution that is compatible with electronically induced nonlinear effects, a femtosecond pump and probe technique is implemented. Probe pulses (signal) with 120 fs-duration and 80 MHz-repetition rate are generated by an optical parameter oscillator at around 1490 nm. The average probe power is kept below 250 nW at the input of the taper. By using such broadband pulses to probe the nanocavity mode, we measure an optical resonance centered at 1491.5 nm with a full width half maximum (FHWM) of 0.6 nm, corresponding to a loaded quality factor of $Q_{loaded} \cong 2485$.

In our experiments, the nonlinear regime is achieved by optically injecting carriers using a 80 MHz-repetition rate, 100 fs-pulse duration Ti:Sa pump source. Pump pulses, emitted at $\lambda = 810$ nm, are absorbed in the InP inducing a carrier population that first relax to the wetting layer bang-edges ($\lambda_{gap} \sim 1.1\ \mu$m). As it has been shown elsewhere [4], this carrier density decreases the refractive index and induces the blue shift of the optical mode. In addition, a slow thermal effect also takes place with a time scale on the order of 1 μs [11]. Therefore, only the averaged thermal loading can be revealed by our measurements which, in turn, can fully resolve the ultrafast changes associated with the carrier dynamics. This was accomplished by analyzing the probe reflectivity/transmission intensity as a function of the delay between the pump and the probe pulses. Time delays are obtained by increasing or decreasing the probe path by means of a computer-controlled translation stage. The delay step is 7 fs, and the maximum positive delay that can be reached is 1.3 ns.

The pump is injected either directly by the surface [see Fig. 1(c)] or multiplexed into the taper [see Fig. 1(d)] in order to achieve all-fibered operation. Both cases are studied in the following sections.

3. Surface Pump

The pump beam is focused down via a 50x, long working distance (20 mm), microscope objective to a diameter of 3.2 μm (@$1/e^2$ of the intensity) shining the structure normally to the 2DPC periodicity.

As the pump power is increased to 0.98 mW, a 3-nm red shift of the resonance is observed for negative or long positive delays ($>$ 1 ns). This red shift, which is associated with thermal effects, becomes a thermal offset for the linear regime. In the following, all (electronically induced) blue shifts are measured from this offset. Such blue shifts are only observed for positives delays [4], [14].

Fig. 2(a) shows the transmitted signal spectra with a pump power of 0.98 mW for different pump-probe delays. A maximum blue shift of 7 nm is obtained near pump-probe coincidence. This is consistent with the fact that the electronic density and the associated blue shift can be assumed to increase within a time of the order of relaxation time of carriers to the conduction and valence band edges ($\sim$1 ps). As the time delay is increased, the blue shift decreases due to carrier recombination. In order to further analyze the temporal behavior and its dependence on the pump power, we measured the spectral shift $\Delta\lambda$ as a function of the pump-probe delay for different pumping powers [see Fig. 2(b)]. A decrease of the total recovery time from (90 ± 20) ps to (30 ± 5) ps (measured at 1/e of the maximum) is observed as the pump power is increased from 0.3 mW to 1 mW [see the inset in Fig. 2(b)]. Both the blue shift and the picosecond time scale are clear signatures of the electronic nature of the nonlinear effect. Furthermore, the decrease of the recovery time with the pump power can be related to nonlinear terms in the carrier recombination process, such as bimolecular recombination [4], which will be studied in detail in Section 5. The observed rise time is of the order of 4 ps (except for the smallest power). As it was shown in [16], this time is related to the photon lifetime in the cavity ($\sim$2 ps).

One interesting application of such ultrafast behavior is to all-optically control and switch a continuous wave (CW) signal. Carrier-induced switching is thus translated into modulation in time at a fixed probe wavelength. In order to test such effects, 490-μW pump pulses are incident from the free space on the surface while the probe is coupled through the taper. The probe is now a CW tunable laser, modulated with 10 MHz repetition rate, pulse duration of 90 ns, and mean power of 235 μW. The

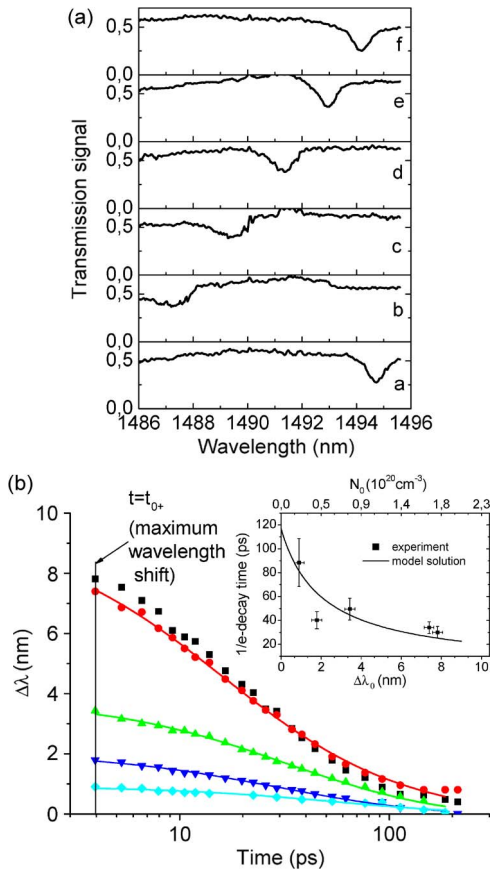

Fig. 2. (a) Transmission spectrum, with a resolution of 0.5 nm, for different pump and probe delays. a) $\Delta t = -24$ ps, b) $\Delta t = 1$ ps, c) $\Delta t = 8$ ps, d) $\Delta t = 25$ ps, e) $\Delta t = 50$ ps, and f) $\Delta t = 140$ ps. The probe power at the entrance of the taper was 20 nW. The pump, with a power of 0.98 mW, is injected by the surface. (b) Resonance shift as a function of the delay time (in logarithmic scale) for different pump powers 0.28 mW (♦), 0.42 mW (▼), 0.54 mW (▲), 0.67 mW (●) and 0.98 mW (■). The rise time is ∼4 ps, except for the smallest power, which is ∼7 ps. Solid lines: Fitted curves using (3) in the text. The fitted parameters are $\tau_{nr} = (0.38 \pm 0.15)$ ns and $\tilde{B} = (6.6 \pm 0.3)$ ns^{-1} nm^{-1} for P = 0.67 mW; $\tau_{nr} = (0.13 \pm 0.03)$ ns and $\tilde{B} = (7 \pm 1)$ ns^{-1} nm^{-1} for P = 0.54 mW; $\tau_{nr} = (0.11 \pm 0.02)$ ns and $\tilde{B} = (14 \pm 2)$ ns^{-1} nm^{-1} for P = 0.42 mW; and $\tau_{nr} = (0.17 \pm 0.1)$ ns and $\tilde{B} = (14 \pm 2)$ ns^{-1} nm^{-1} for P = 0.28 mW. Inset: Dependence of the decay time (Δt at 1/e) on the initial wavelength shift. Solid line: Model solution for the decay time from (4), using the weighted average of the fitted parameters in (b), namely, $\langle \tilde{B} \rangle = 6.74$ ns$^{-1} \cdot$ nm^{-1} and $\langle \tau_{nr} \rangle = 0.117$ ns.

modulation was implemented to measure the signal contrast. Time traces are measured using a 1.44-GHz bandwidth avalanche photodetector (APD). Fig. 3(a) shows the time trace of the transmitted signal for two different wavelengths. The periodicity of 12.5 ns corresponds to the pump repetition rate. Clearly, in the presence of the pump pulses the transmitted signal drops or increases, depending on whether the probe wavelength is blue or red-shifted with respect to the cavity resonance, respectively. This is summarized in Fig. 3(b), which shows the variation of the transmitted peak amplitude as a function of the probe wavelength (black) superimposed on the resonance spectrum (red). A contrast as high as 20% is achieved as the probe is slightly shifted but close to the minimum of the resonance [see Fig. 3(b)]. This is a factor ∼2 smaller than the contrast of the resonance in transmission, which can be attributed to the limited bandwidth of the APD, resulting in a time convolution of the actual signal.

4. Fibered Pump

All-fibered switching capabilities are studied by injecting both the 100-fs-long, 810-nm pump pulses and the 120-fs-long, 1490-nm signal pulses into the taper. The pump power at the input of the fiber

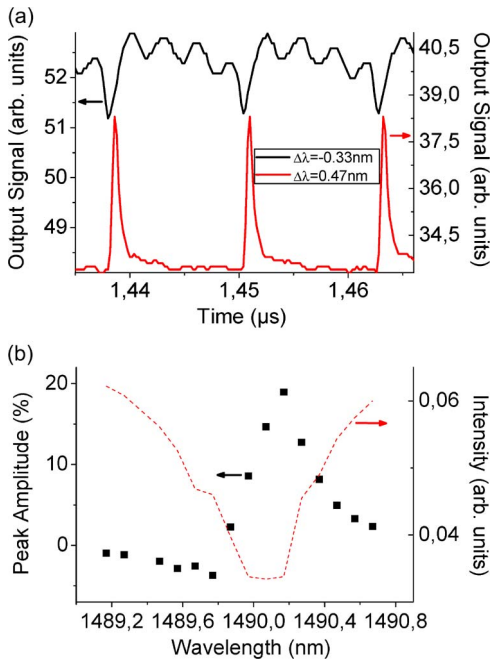

Fig. 3. (a) Time-resolved transmission, at a resolution 1 ns, for $\Delta\lambda$ $(\lambda_{inj} - \lambda_{res}) = -0.33$ nm (black) and $\Delta\lambda = 0.47$ nm (red), where each peak corresponds to the arrival of one pump pulse $(\Delta t \sim 12.5$ ns). (b) Transmitted amplitude spectrum in % with respect to the background signal (■) and cavity resonance (dash line).

is fixed to ∼2.5 mW, whereas the probe is kept below 250 μW to avoid probe-induced nonlinearities. Note that these values are measured at the input of the fiber and the actual pump and signal powers near the cavity are lowered due to both contact and propagation losses in the taper.

The reflected signal spectrum is represented in Fig. 4(a) for different pump-probe delays. A maximum blue shift of 0.9 nm is obtained for the pump-probe coincidence. The linear resonance in this case is at 1494.3 nm. Although it is difficult to evaluate the actual pump intensity acting in the nanocavity region, an order of magnitude can be estimated from the pumping powers in the two configurations (free space and fiber coupled), giving the same blue shift. Indeed, the blue shift achieved in the fibered pumping configuration (∼1 nm) is close to the one obtained in the surface-pumping configuration for a pump power of 0.28 mW [see Fig. 2(b), (♦)]. Therefore, the pumping level in the fibered configuration is equivalent to ∼0.28 mW shining the surface. As the InP coefficient of absorption at 810 nm is ∼33% and considering the cavity surface with respect to the excitation surface, the absorbed pump power in the cavity region is reduced to ∼10 μW of the same order of magnitude as in [14].

We now consider the dynamical features in the fibered configuration. Fig. 4(b) shows the time dependence of the blue shift in the experimental conditions of Fig. 4(a). The rise time (switch ON) is ∼20 ps, and the decay time (switch OFF) is (170 ±15) ps. These times are in the picosecond time scale and are attributed to the carrier-induced refractive index change, as previously. However, they are longer compared with the ones measured in the surface-pump configuration. In both cases, the signal is fiber coupled, and there is no measurable effect associated with the signal intensity. Therefore, the increased ON and OFF times can be related to a linear and/or nonlinear dispersion of the pump pulses in the fiber and the taper. In order to verify this, we further investigate the origin of the increase of the ON/OFF characteristic times as follows. First, we implement an autocorrelation measurement of the 100 fs-pulses at the output of a 7-m-long single mode fiber, which is equivalent to the propagation length of a pulse before reaching the taper in the fibered-pump setup. We find that pump pulses of 3 mW are stretched to ∼7 ps [see the inset in Fig. 4(b)]. This duration does not significantly change for all the pump pulse energies considered in the switching configuration. Next,

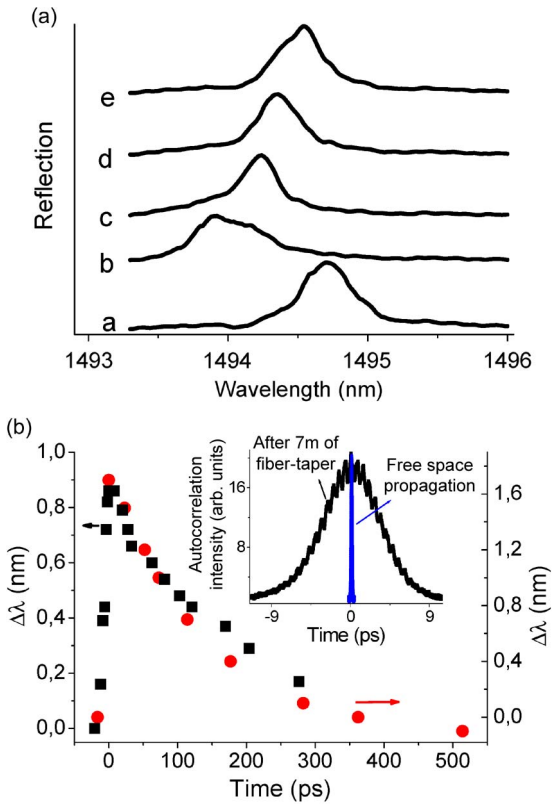

Fig. 4. (a) All fibered configuration. Reflectivity intensity for different pump and probe delays: a) $\Delta t = -21$ ps, b) $\Delta t = 21$ ps, c) $\Delta t = 100$ ps, d) $\Delta t = 170$ ps, e) $\Delta t = 277$ ps, with a vertical offset and resolution 0.05 nm. The pump power was 2.5 mW at the input of the fiber. (b) Resonance shift as a function of pump-probe delays for all-fibered configuration (■) (decay time at $1/e = 170$ ps and rise time 20 ps) and for surface pumping with 7-pump pulses duration (•) (decay and rise times: 115 ps and 20 ps, respectively). Inset: Autocorrelation measurement of pump pulses; free space propagation (blue line) and after 7 m of a single mode fiber (black line).

we implement a surface pumping configuration with 7 ps-pump pulses duration in the following way: The pump pulses are temporally broaden to ∼7 ps by taking benefit from the chromatic dispersion after propagating through a 7-m-long fiber and eventually sent to the sample in the same surface-pumping conditions of Fig. 2. The measured rise and decay times are now ∼20 ps and (115 ± 20) ps, respectively [see Fig. 4(b) (•)]. The rise time is close to the one measured in the all-fiber coupling configuration, whereas the decay time overlaps with the one obtained in the femtosecond surface pumping experiment for the same blue shift: (90 ± 20) ps. This builds confidence on the fact that the stretching of the pump pulses is at the origin of the increase of the ON response. Indeed, by contrast with the 100-fs pump pulse in the surface-pumping configuration, which is shorter than all time scales of the system leading to free carrier relaxation, the 7-ps duration pump pulse is longer compared to the photon lifetime and approaches the fast carrier recombination time. The 20-ps rise time can thus be understood as resulting from the longer pumping pulse driving the system. However, the increase of the decay time in the fibered pump configuration with respect to surface pumping is more intriguing and could be related to a lower carrier density within the WL when pumping through the fiber, as will be discussed in the next section.

5. Discussion

In this section, we discuss the origin of the ultrafast switching dynamics obtained through femtosecond pump and probe experiments. Since the pump-induced effects shift the resonance to

the blue side of the spectrum, the leading nonlinear effect is to decrease the refractive index. Therefore, the nonlinearities in play are mainly of electronic origin, i.e., they come from carrier-induced effects, which turn out to be dominant against (fast) red-shift processes, such as intrinsic Kerr effects. The injected carrier density in the surface pump experiment, as deduced from the experimental conditions, is typically $N_{2D} \sim 10^{14}$ cm^{-2} within the PhC slab, corresponding to an overall 3-D density of $N_{3D} \sim 5\ 10^{18}$ cm^{-3} injected carriers. Considering carrier diffusion in the InP, which is essentially governed by holes ($D_h \sim 5$ cm^2/s), carriers are able to reach the wetting layer (WL) in $\sim(100\ \text{nm})^2/D_h \approx 20$ ps; therefore, only a fraction of the total carriers accounting for fast carriers will be eventually captured inside the WL in a time shorter than 20 ps. Such a fraction will be considered as a fitting parameter in our analysis.

We now analyze and compare the carrier-induced effects of each semiconductor structure. For probe photon energies ($h\nu$) close enough to the bandgap energies (approximately $(E_g - h\nu)/E_g < 0.15$ for a III–V semiconductor), it has been shown that index change is dominated by band-filling effects [17], which is indeed the case of the QDs in our system. On the other hand, for very low photon energies with respect to the electronic bandgaps $h\nu \ll E_g$, as is the case of the InP, Drude effects are dominant. In the case of the wetting layer (WL), we can expect both band filling and Drude effects contributing to the decrease of refractive index.

The refractive index change due to Drude effects for carrier densities close to transparency values ($N_{tr} \sim 10^{18}$ cm^{-3}) can be estimated as large as $\Delta n/n \sim 0.001$ [17], leading to wavelength shifts of about $\Delta\lambda \sim \lambda\Delta n/n \sim 1$ nm. Band-filling effects produce stronger refractive index changes for a carrier density $N \sim N_{tr}$, both in bulk materials and in quantum wells (QWs). For instance, in InAsP/InP QWs, we have previously observed $\Delta n/n \sim 0.01$ for carrier densities close to QW transparency ($N_{2D} \sim 10^{12}$ cm^{-2}) [4], [7]. In the case of QDs, however, the maximum carrier density that can be injected equals the QD density $N_{QD} \sim 10^{10}$ cm^{-2}. Taking into account that this remains at least two orders of magnitude below the carrier density in the WL, we can therefore conclude that refractive index change in the QDs, even if all the QD levels are occupied, can be neglected with respect to index change induced by carriers in the WL. Electronic nonlinearities in the QDs could be tested by pumping at a longer wavelength (e.g., 1.3 μm) or even through degenerated pump and probe experiments. From now on, we thus consider that the nonlinear carrier-induced effects are produced by a carrier density confined within the WL. Furthermore, we assume that the refractive index change, hence the wavelength shift, can be considered to be a linear function of the carrier density

$$\Delta\lambda = \Delta\lambda_N N \tag{1}$$

where $\Delta\lambda_N$ is taken constant and N is the 3-D carrier density. Therefore, the dynamics of the wavelength shift $\Delta\lambda(t)$ is considered proportional to the carrier dynamics N(t).

We then study the carrier dynamics governing the observed time dependence of the wavelength shift [see Fig. 2(b)]. Two main recombination processes can be taken into account: a nonradiative recombination process with a time constant τ_{nr} and a radiative recombination process or bimolecular recombination at a rate BN, B being the bimolecular recombination coefficient, which is expected to play an important role especially for high carrier densities. The corresponding rate equation for N(t) is

$$\frac{dN}{dt} = -\frac{N}{\tau_{nr}} - BN^2. \tag{2}$$

We solve (2) analytically for femtosecond pumping. In such a case, carriers relax freely from an initial carrier density $N(t = t_{0+}) = N_0$ injected by the femtosecond pumping pulse centered at $t = t_0$, which has already been described as a kick-like pumping process [16], [18]. Defining $\Delta t = t - t_{0+}$, the solution of (2) reads

$$N(\Delta t) = \frac{N_0 e^{-\Delta t/\tau_{nr}}}{1 + B\tau_{nr}N_0(1 - e^{-\Delta t/\tau_{nr}})}. \tag{3}$$

The decay time $\tau_{1/e}$ defined as the time for the decay of the carrier density at 1/e of the initial value, $N(\Delta t = \tau_{1/e}) = N_0/e$, can be readily found from (3) as

$$\tau_{1/e} = \tau_{nr} \ln\left(\frac{e + B\tau_{nr}N_0}{1 + B\tau_{nr}N_0}\right). \quad (4)$$

Note that in the limit $BN_0 \ll (\tau_{nr})^{-1}$ we obtain $\tau_{1/e} \to \tau_{nr}$, meaning that for small bimolecular recombination rates, the nonradiative decay time is dominant.

Equations (3) and (4) can be re-written in terms of the (experimentally measured) initial wavelength shift $(\Delta\lambda_0)$ by evaluating (1) at $t = t_{0+}$, which gives $N_0 = \Delta\lambda_0/\Delta\lambda_N$. Using this, we have fitted (3) to the experimental data in Fig. 2(b) with the fitting parameters $\widetilde{B}$, $\Delta\lambda_0$ and τ_{nr}, where $\widetilde{B} \equiv B/\Delta\lambda_N$. We notice that for the highest pump power $P = 0.98$ mW, the dynamics of $\Delta\lambda$ almost superimpose to those for $P = 0.67$ mW, meaning that carrier saturation is playing an important role, and therefore, no additional information can be obtained from the data corresponding to $P = 0.98$ mW. The excellent quality of the fits can be observed in Fig. 2(b). We average out the parameter values resulting from fitting the four curves in Fig. 2(b) using a weighted average procedure. Normalized weights are defined assuming an ensemble of four independent measurements with weights w_i as usual, i.e., $w_i = (e_i^2 \sum 1/e_i^2)^{-1}$, where e_i is the standard deviation of the ith fitted value. The weighted average gives $\langle\widetilde{B}\rangle = (6.7 \pm 1)\ \text{ns}^{-1} \cdot \text{nm}^{-1}$ and $\langle\tau_{nr}\rangle = (0.12 \pm 0.03)$ ns, where the errors are given by the weighted standard deviation. The obtained nonradiative recombination time in this system is of the same order of magnitude as in previous measurements of 2DPC samples with InAsP/InP QWs [4]. The accuracy of these two fitted parameters can be tested by comparing the experimental decay times with those obtained using (4). This is shown in Fig. 2(b) (inset). It can be observed that the dependency of the decay times on the initial carrier density is well reproduced by (4) with the two averaged parameters $\langle\widetilde{B}\rangle$ and $\langle\tau_{nr}\rangle$.

In order to relate $\langle\widetilde{B}\rangle$ to the physical coefficient B, $\Delta\lambda_N$ has to be found. With this aim, we first calculate the injected carrier density in the WL as a function of (small) pump power, $N_{0,WL} = fT\alpha_0 LP/dh\nu_p A$, where f is the probability of carrier capture in the WL after diffusion, T is the pulse period of the femtosecond pulse-train, L is the membrane thickness, d is the WL thickness $(d = 0.6\ \text{nm})$, $h\nu_p$ is the pump photon energy, A is the surface of the pumped region ($A = \pi r^2$, with $r = 1.6\ \mu$m), and α_0 is the linear absorption coefficient at the pump wavelength $(\alpha_0 L \sim 0.4)$. Next, we relate the wavelength shift to the pump power for small P: $\Delta\lambda_0 \sim 3.2$ nm/mW P. As a result, $\Delta\lambda_N \sim (d/f) \times 1.3\ 10^{-14}\ \text{nm} \cdot \text{cm}^2$. Using an already reported value for the bimolecular recombination coefficient in InP-based materials, i.e., $B \sim 3\ 10^{-10}\ \text{cm}^3/\text{s}$ [18], the fraction of the total carrier population within the WL becomes $f \sim 0.02$. Considering that the remaining (1-f) carriers are within the InP, the ratio of the density in the InP to that in the WL is $N_{0,InP}/N_{0,WL} \sim d(1-f)/Lf \sim 0.1$, meaning that even for such small fraction f, the carrier density in the WL is one order of magnitude larger than the density in the bulk. This justifies our early assumption that the main contribution of carrier-induced effects comes from the WL. In addition, we point out that the small fraction of the carrier density trapped within the WL in the observation time scale could be explained as a result of the rather slow diffusion time of holes across the membrane estimated above (~20 ps).

As pointed out in Section 4, in the case of the fibered pump configuration, the observed relaxation time of an initial wavelength shift of $\Delta\lambda_0 \sim 1$ nm is ~170 ps, whereas that for the same $\Delta\lambda_0$ in the surface configuration is ~90 ps. This could be explained under the hypothesis of a lower carrier density inside the WL in the fibered pump configuration, which might be related to a different pumped volume in this case with respect to free space pumping. Indeed, carriers are mostly injected close to the membrane surface in contact with the taper rather than throughout the whole membrane thickness as in the free space illumination. We can thus expect a smaller fraction of carriers being captured by the WL and, therefore, a weaker bimolecular recombination effect leading to a slower decay time. The fact that a smaller carrier density in the WL for the fiber-pumping configuration gives the same $\Delta\lambda_0$ as in the surface pumping configuration could be explained as an additional blue shift induced by the remaining (1-f) carriers in the InP.

It is worth pointing out that radiative recombination governs carrier dynamics for the highest pumping powers used in this work. In particular, they are responsible for the shortest times that have been observed, that is, on the order of 30 ps, corresponding to the largest carrier densities. Also, since carrier saturation effects appear for $P > 0.7$ mW, it can be inferred that for the shortest observed time of 30 ps, a material limit is attained for ultrafast carrier-induced switching processes in this class of systems. Notice that the shortest relaxation times observed here are of the same order of magnitude as those recently obtained in resonantly pumped H0 cavities where carrier diffusion plays a main role in carrier relaxation due to the small optical volume of the H0 cavity [19].

6. Conclusion

We have performed time-resolved pump and probe measurements with femtosecond resolution of the optical response of an active 2DPC nanocavity to investigate its switching capabilities. The signal is evanescently coupled through a fibered taper, and the pump is either sent by the surface or through the tapered fiber. The optical pump provides ON/OFF switching of the transmitted or reflected signals with time features associated with the electronically induced nonlinearity. In the case of fiber-coupled pump pulses configuration, an all-fibered stable operation is achieved at the expense of increased ON and OFF switching times up to 20 ps and 170 ps, respectively. These values are still shorter by one order of magnitude than the previously reported ON/OFF switching times [14]. Through fitting the decay time of the nonlinear effect by means of a rate equation for the carrier density, we have explained the origin of the shortest relaxation times (30 ps) as a result of radiative carrier recombination inside the wetting layer. Moreover, we have shown that the increase of the rise time in the all-fibered configuration is a consequence of pump-pulse dispersion in the fiber. This could be pre-compensated at the input of the tapered fiber in order to retrieve the characteristic times measured in the surface pumping configuration, that is, ON times as short as 4 ps. In addition to the switching capabilities, these kinds of PC cavities with embedded QDs could be used as laser sources with ultrafast tunability of the laser mode, taking benefit from the large carrier-induced nonlinear effects in the wetting layer described in this work.

Acknowledgment

The authors would like to thank G. Patriarche and A. Beveratos for helpful discussions.

References

[1] C. Soukoulis, *Photonic Crystals and Light Localization in the 21st Century*. Boston, MA: Kluwer, 2001.
[2] H. Nakamura, Y. Sugimoto, K. Kanamoto, N. Ikeda, Y. Tanaka, Y. Nakamura, S. Ohkouchi, Y. Watanabe, K. Inoue, H. Ishikawa, and K. Asakawa, "Ultra-fast photonic crystal/quantum dot all-optical switch for future photonic networks," *Opt. Express*, vol. 12, no. 26, pp. 6606–6614, Dec. 2004.
[3] A. D. Bristow, J.-P. R. Wells, W. H. Fan, A. M. Fox, M. S. Skolnick, D. M. Whittaker, A. Tahraoui, T. F. Krauss, and J. S. Roberts, "Ultrafast nonlinear response of AlGaAs two-dimensional photonic crystal waveguides," *Appl. Phys. Lett.*, vol. 83, no. 5, pp. 851–853, Aug. 2003.
[4] F. Raineri, C. Cojocaru, P. Monnier, J. A. Levenson, R. Raj, C. Seassal, X. Letartre, and P. Viktorovitch, "Ultrafast dynamics of the third-order nonlinear response in a two-dimensional InP-based photonic crystal," *Appl. Phys. Lett.*, vol. 85, no. 11, pp. 1880–1882, Sep. 2004.
[5] J. F. Holzman, P. Strasser, R. Wüest, F. Robin, D. Erni, and H. Jäckel, "Picosecond free-carrier recombination in indium phosphide photonic crystals," in *Proc. Int. Conf. Indium Phosphide Related Mater.*, 2005, pp. 570–573.
[6] C. Husko, A. De Rossi, S. Combrié, Q. V. Tran, F. Raineri, and C. W. Wong, "Ultrafast all-optical modulation in GaAs photonic crystal cavities," *Appl. Phys. Lett.*, vol. 94, no. 2, p. 021111, Jan. 2009.
[7] A. Yacomotti, F. Raineri, G. Vecchi, P. Monnier, R. Raj, J. A. Levenson, B. Ben Bakir, C. Seassal, X. Letartre, P. Viktorovitch, L. Di Cioccio, and J.-M. Fedeli, "All-optical bistable band-edge Bloch modes in a two-dimensional photonic crystal," *Appl. Phys. Lett.*, vol. 88, no. 23, p. 231107, Jun. 2006.
[8] T. Tanabe, M. Notomi, S. Mitsugi, A. Shinya, and E. Kuramochi, "All-optical switches on a silicon chip realized using photonic crystal nanocavities," *Appl. Phys. Lett.*, vol. 87, no. 15, p. 151112, Oct. 2005.
[9] A. Yacomotti, F. Raineri, G. Vecchi, I. Sagnes, M. Strassner, L. Le Gratiet, R. Raj, and A. Levenson, "Ultrafast nonlinear response around 1.5 μm in 2D AlGaAs/AlOx photonic crystal," *Appl. Phys. B, Photophys. Laser Chem.*, vol. 81, no. 2/3, pp. 333–336, Jul. 2005.
[10] I. Hwang, S. Kim, J. Yang, S. Kim, S. Lee, and Y. Lee, "Curved-microfiber photon coupling for photonic crystal light emitter," *Appl. Phys. Lett.*, vol. 87, no. 13, p. 131 107, Sep. 2005.

[11] M. Brunstein, R. Braive, R. Hostein, A. Beveratos, I. Robert-Philip, I. Sagnes, P. Monnier, T. Karle, F. Raineri, A. M. Yacomotti, J. A. Levenson, V. Moreau, G. Tessier, and Y. De Wilde, "Thermo-optical dynamics in an optically pumped Photonic Crystal nano-cavity," *Opt. Express*, vol. 17, no. 19, pp. 17 118–17 129, Sep. 2009.
[12] P. E. Barclay, K. Srinivasan, M. Borselli, and O. Painter, "Probing the dispersive and spatial properties of photonic crystal waveguides via highly efficient coupling from fiber tapers," *Appl. Phys. Lett.*, vol. 85, no. 1, pp. 4–6, Jul. 2004.
[13] C. Grillet, C. Smith, D. Freeman, S. Madden, B. Luther-Davies, E. C. Magi, D. J. Moss, and B. J. Eggleton, "Efficient coupling to chalcogenide glass photonic crystal waveguides via silica optical fiber nanowires," *Opt. Express*, vol. 14, no. 3, pp. 1070–1078, Feb. 2006.
[14] I. Hwang, M. Kim, and Y. Lee, "All-optical switching in InGaAsP–InP photonic crystal resonator coupled with microfiber," *IEEE Photon. Technol. Lett.*, vol. 19, no. 19, pp. 1535–1537, Oct. 2007.
[15] Y. Akahane, T. Asano, B.-S. Song, and S. Noda, "High-Q photonic nanocavity in a two-dimensional photonic crystal," *Nature*, vol. 425, no. 6961, pp. 944–947, Oct. 2003.
[16] A. Yacomotti, F. Raineri, G. Cojucaru, P. Monnier, J. A. Levenson, and R. Raj, "Nonadiabatic dynamics of the electromagnetic field and charge carriers in high-Q photonic crystal resonators," *Phys. Rev. Lett.*, vol. 96, no. 9, p. 093 901, Mar. 2006.
[17] J. P. Mondia, H. W. Tan, S. Linden, H. M. van Driel, and J. F. Young, "Ultrafast tuning of two-dimensional planar photonic-crystal waveguides via free-carrier injection and the optical Kerr effect," *J. Opt. Soc. Amer. B, Opt. Phys.*, vol. 22, no. 11, pp. 2480–2486, Nov. 2005.
[18] F. Raineri, A. M. Yacomotti, T. J. Karle, R. Hostein, R. Braive, A. Beveratos, I. Sagnes, and R. Raj, "Dynamics of band-edge photonic crystal lasers," *Opt. Express*, vol. 17, no. 5, pp. 3165–3172, Mar. 2009.
[19] K. Nozaki, T. Tanabe, A. Shinya, S. Matsuo, T. Sato, H. Taniyama, and M. Notomi, "Sub-femtojoule all optical switching using a photonic-crystal nanocavity," *Nature Photon.,* May 2, 2010. DOI: 10.1038/nphoton.2010.89.